

SEARCH FOR GAMMA RAY BURSTS WITH THE ARGO-YBJ DETECTOR IN SCALER MODE

G. Aielli^{1,2}, C. Bacci^{3,4}, F. Barone^{5,6}, B. Bartoli^{6,7}, P. Bernardini^{8,9}, X.J. Bi¹⁰, C. Bleve^{8,9}, P. Branchini⁴, A. Budano⁴, S. Bussino^{3,4}, A.K. Calabrese Melcarne^{8,9,+}, P. Camarri^{1,2}, Z. Cao¹⁰, A. Cappa^{11,12}, R. Cardarelli², S. Catalanotti^{6,7}, C. Cattaneo¹³, S. Cavaliere^{6,7}, P. Celio^{3,4}, S.Z. Chen¹⁰, N. Cheng¹⁰, P. Creti⁹, S.W. Cui¹⁴, B.Z. Dai¹⁵, G. D'Alí Staiti^{16,17}, Danzengluobu¹⁸, M. Dattoli^{11,12,19}, I. De Mitri^{8,9}, R. De Rosa^{6,7}, B. D'Ettorre Piazzoli^{6,7}, M. De Vincenzi^{3,4}, T. Di Girolamo^{6,7}, X.H. Ding¹⁸, G. Di Sciascio², C.F. Feng²⁰, Zhaoyang Feng¹⁰, Zhenyong Feng²¹, F. Galeazzi⁴, P. Galeotti^{11,19}, X.Y. Gao¹⁵, R. Gargana⁴, F. Garufi^{6,7}, Q.B. Gou¹⁰, Y.Q. Guo¹⁰, H.H. He¹⁰, Haibing Hu¹⁸, Hongbo Hu¹⁰, Q. Huang²¹, M. Iacovacci^{6,7}, R. Iuppa^{1,2}, I. James^{3,4}, H.Y. Jia²¹, Labaciren¹⁸, H.J. Li¹⁸, J.Y. Li²⁰, B. Liberti², G. Liguori^{13,22}, C.Q. Liu¹⁵, J. Liu¹⁵, H. Lu¹⁰, G. Mancarella^{8,9}, S.M. Mari^{3,4}, G. Marsella^{9,23}, D. Martello^{8,9}, S. Mastroianni⁶, X.R. Meng¹⁸, J. Mu¹⁵, C.C. Ning¹⁸, L. Palummo^{1,2}, M. Panareo^{9,23}, L. Perrone^{9,23}, P. Pistilli^{3,4}, X.B. Qu²⁰, E. Rossi⁶, F. Ruggieri⁴, L. Saggese^{6,7}, P. Salvini¹³, R. Santonico^{1,2}, A. Segreto^{16,24}, P.R. Shen¹⁰, X.D. Sheng¹⁰, F. Shi¹⁰, C. Stanescu⁴, A. Surdo⁹, Y.H. Tan¹⁰, P. Vallania^{11,12,*}, S. Vernetto^{11,12}, C. Vigorito^{11,19}, H. Wang¹⁰, Y.G. Wang¹⁰, C.Y. Wu¹⁰, H.R. Wu¹⁰, B. Xu²¹, L. Xue²⁰, H.T. Yang¹⁵, Q.Y. Yang¹⁵, X.C. Yang¹⁵, G.C. Yu²¹, A.F. Yuan¹⁸, M. Zha¹⁰, H.M. Zhang¹⁰, J.L. Zhang¹⁰, L. Zhang¹⁵, P. Zhang¹⁵, X.Y. Zhang²⁰, Y. Zhang¹⁰, Zhaxisangzhu¹⁸, X.X. Zhou²¹, F.R. Zhu¹⁰, Q.Q. Zhu¹⁰,

and

G. Zizzi^{8,9}

*Corresponding author: Piero.Vallania@to.infn.it

¹Dipartimento di Fisica dell’Università “Tor Vergata” di Roma, via della Ricerca Scientifica 1, 00133 Roma, Italy.

²Istituto Nazionale di Fisica Nucleare, Sezione di Tor Vergata, via della Ricerca Scientifica 1, 00133 Roma, Italy.

³Dipartimento di Fisica dell’Università “Roma Tre” di Roma, via della Vasca Navale 84, 00146 Roma, Italy.

⁴Istituto Nazionale di Fisica Nucleare, Sezione di Roma3, via della Vasca Navale 84, 00146 Roma, Italy.

⁵Dipartimento di Scienze Farmaceutiche dell’Università di Salerno, via Ponte Don Melillo, 84084 Fisciano (SA), Italy.

⁶Istituto Nazionale di Fisica Nucleare, Sezione di Napoli, Complesso Universitario di Monte Sant’Angelo, via Cinthia, 80126 Napoli, Italy.

⁷Dipartimento di Fisica dell’Università di Napoli, Complesso Universitario di Monte Sant’Angelo, via Cinthia, 80126 Napoli, Italy.

⁸Dipartimento di Fisica dell’Università del Salento, via per Arnesano, 73100 Lecce, Italy.

⁹Istituto Nazionale di Fisica Nucleare, Sezione di Lecce, via per Arnesano, 73100 Lecce, Italy.

¹⁰Key Laboratory of Particle Astrophysics, Institute of High Energy Physics, Chinese Academy of Science, P.O. Box 918, 100049 Beijing, P.R. China.

¹¹Istituto Nazionale di Fisica Nucleare, Sezione di Torino, via P.Giuria 1 - 10125 Torino, Italy.

¹²Istituto di Fisica dello Spazio Interplanetario dell’Istituto Nazionale di Astrofisica, corso Fiume 4 - 10133 Torino, Italy.

¹³Istituto Nazionale di Fisica Nucleare Sezione di Pavia, via Bassi 6, 27100 Pavia, Italy.

¹⁴Hebei Normal University, Shijiazhuang 050016, Hebei, P.R. China.

Received _____; accepted _____

¹⁵Yunnan University, 2 North Cuihu Rd, 650091 Kunming, Yunnan, P.R. China.

¹⁶Istituto Nazionale di Fisica Nucleare, Sezione di Catania, Viale A. Doria 6 - 95125 Catania, Italy.

¹⁷Università degli Studi di Palermo, Dipartimento di Fisica e Tecnologie Relative, Viale delle Scienze, Edificio 18 - 90128 Palermo, Italy.

¹⁸Tibet University, 850000 Lhasa, Xizang, P.R. China.

¹⁹Dipartimento di Fisica Generale dell'Università di Torino, via P.Giuria 1 - 10125 Torino, Italy.

²⁰Shandong University, 250100 Jinan, Shandong, P.R. China

²¹South West Jiaotong University, 610031 Chengdu, Sichuan, P.R. China.

²²Dipartimento di Fisica Nucleare e Teorica dell'Università di Pavia, via Bassi 6, 27100 Pavia, Italy.

²³Dipartimento di Ingegneria dell'Innovazione, Università del Salento, Via per Monteroni, 73100 Lecce, Italy.

²⁴Istituto di Astrofisica Spaziale e Fisica Cosmica di Palermo, Istituto Nazionale di Astrofisica, Via Ugo La Malfa 153 - 90146 Palermo, Italy.

⁺Presently at INFN-CNAF, Bologna, Italy

ABSTRACT

We report on the search for Gamma Ray Bursts (GRBs) in the energy range 1-100 GeV in coincidence with the prompt emission detected by satellites using the Astrophysical Radiation with Ground-based Observatory at YangBaJing (ARGO-YBJ) air shower detector. Thanks to its mountain location (Yangba-jing, Tibet, P.R. China, 4300 m a.s.l.), active surface (~ 6700 m² of Resistive Plate Chambers), and large field of view (~ 2 sr, limited only by the atmospheric absorption), the ARGO-YBJ air shower detector is particularly suitable for the detection of unpredictable and short duration events such as GRBs. The search is carried out using the “single particle technique”, i.e. counting all the particles hitting the detector without measurement of the energy and arrival direction of the primary gamma rays.

Between 2004 December 17 and 2009 April 7, 81 GRBs detected by satellites occurred within the field of view of ARGO-YBJ (zenith angle $\theta \leq 45^\circ$). It was possible to examine 62 of these for > 1 GeV counterpart in the ARGO-YBJ data finding no statistically significant emission. With a lack of detected spectra in this energy range fluence upper limits are profitable, especially when the redshift is known and the correction for the extragalactic absorption can be considered. The obtained fluence upper limits reach values as low as 10^{-5} erg cm⁻² in the 1-100 GeV energy region.

Besides this individual search for a higher energy counterpart, a statistical study of the stack of all the GRBs both in time and in phase was made, looking for a common feature in the GRB high energy emission. No significant signal has been detected.

Subject headings: gamma rays: bursts — gamma rays: observations

1. INTRODUCTION

Over the past ten years, a considerable effort has been made to study Gamma Ray Bursts (GRBs). The solution of the puzzle about their distance by the BeppoSAX satellite in 1997 with the detection of the first afterglow (Costa et al. 1997) was followed by a small fleet of satellites (Swift, HETE, AGILE, and now the Fermi Gamma Ray Space Telescope) that performed an extensive study in the keV-MeV energy range. At ground level, air shower detectors can contribute to the study of the energy region ≥ 1 GeV using the “single particle technique” (Veronetto 2000), i.e. counting all the particles hitting the detector without measurement of the energy and arrival direction of the primary gamma rays. The processes leading to the detection of Very High Energy (VHE) radiation (extending between 1 GeV and 1 TeV) from a GRB start with the acceleration of the parent particles. Since the models predicting the production of gamma rays in this energy range are both leptonic and hadronic, the maximum energy of electrons and protons is linked to the fireball parameters (Fox & Mészáros 2006). Once the parent particles have been accelerated, the VHE gamma rays can result from several production processes - mainly inverse Compton scattering by electrons, electron and proton synchrotron emission, and photon-pion production - each of them included in a wide variety of theoretical models with different hypotheses on the production region, giving different features of the emitted signal (see for example the review article by Mészáros (2006) and references therein). Once produced, the VHE radiation suffers absorption either in the source itself or in the Extragalactic Background Light (EBL) before reaching the Earth (Salamon & Stecker 1998; Totani 2000). The detected signal is thus the overlap of the previous mechanisms, that are difficult to disentangle; nevertheless the measurements in this energy range can be used as a test for the competing models. In particular, the detection of VHE gamma rays and the measurement of the cutoff energy in the GRB spectrum could provide valuable clues to the baryon content, Lorentz factor, and ambient magnetic field of the relativistic fireball. No

cutoff energy has been detected so far by satellites up to 1 GeV, forcing the search into more energetic regions. The energy range between 1 and 100 GeV is particularly interesting since the absorption of high energy gamma rays by the EBL becomes relevant above this region, limiting the possibility of detection to nearby objects while most of the observed GRBs occurs at large redshifts. Anyway the knowledge of the EBL is still poor and the problem of the opacity of the Universe to gamma rays in the sub-TeV energy range still open (e.g. Albert et al. 2008; Stecker & Scully 2009).

In the 1-100 GeV energy region, the detection by EGRET of only 3 GRBs (Catelli et al. 1997) during 7 years of observations indicates that their spectra are usually soft. Recently, the Large Area Telescope (LAT) on board the Fermi Gamma Ray Space Telescope announced the detection of more than 10 photons above 1 GeV from GRB080916C (Tajima et al. 2008) and of emission up to 3 GeV from GRB081024B (Omodei et al. 2008) (unfortunately both these events were below the horizon of our detector). At higher energies, hints ($\sim 3\sigma$) of emissions detected at ground level have been reported by Milagrito for GRB970417A ($E > 650$ GeV) (Atkins et al. 2000) and by the GRAND array for GRB971110 ($E > 10$ GeV) (Poirier et al. 2003). A marginal emission for GRB920925C was also reported by HEGRA AIROBICC ($E > 20$ TeV) (Padilla et al. 1998), while the Tibet Air Shower array found an indication of 10 TeV emission in a stacked analysis of 57 bursts (Amenomori et al. 1996).

Forty years after their discovery, and more than ten years after the detection of the first afterglow by BeppoSAX, the physical origin of the enigmatic GRBs is still under debate. The scarcity of information generates a confused situation, allowing a great variety of very different models. In these conditions, and mainly in the > 1 GeV energy region, any result could be of great importance to approach the solution of the GRB mystery.

In this paper, the search for emission in the 1-100 GeV range in coincidence with the prompt emission detected by satellites is presented for several GRBs.

2. THE DETECTOR

The Astrophysical Radiation with Ground-based Observatory at YangBaJing (ARGO-YBJ) is an extensive air shower detector located at an altitude of 4300 m a.s.l. (corresponding to a vertical atmospheric depth of 606 g cm^{-2}) at the Yangbajing Cosmic Ray Laboratory (30.11°N , 90.53°E). The detector is composed of a single layer of Resistive Plate Chambers (RPCs), operated in streamer mode (Aielli et al. 2006) and grouped into 153 units called “clusters” ($5.7 \times 7.6 \text{ m}^2$). Each cluster is made up of 12 RPCs ($1.225 \times 2.850 \text{ m}^2$) and each RPC is read out by using 10 pads, with dimensions $55.6 \times 61.8 \text{ cm}^2$, representing the space-time pixels of the detector. The clusters are disposed in a central full coverage carpet (130 clusters, $\sim 5600 \text{ m}^2$, $\sim 93\%$ of active surface) and a sampling guard ring ($\sim 40\%$ of coverage) in order to increase the effective area and improve the core location reconstruction.

The detector is connected to two independent data acquisition systems, corresponding to the shower and scaler operation modes.

In shower mode the arrival time and location of each particle are recorded using the “pads”. The present trigger threshold is set to 20 fired pads, corresponding to an energy threshold for photons of a few hundred GeV and a trigger rate of $\sim 3.8 \text{ kHz}$.

In scaler mode the total counts are measured every 0.5 s: for each cluster the signal coming from its 120 pads, representing the counting rate on a surface of $\sim 43 \text{ m}^2$, is added up and put in coincidence in a narrow time interval (150 ns), giving the counting rates of ≥ 1 , ≥ 2 , ≥ 3 , and ≥ 4 pads, that are read by four independent scaler channels. These counting rates are referred in the following respectively as $C_{\geq 1}$, $C_{\geq 2}$, $C_{\geq 3}$, and $C_{\geq 4}$, and the corresponding rates are $\sim 40 \text{ kHz}$, $\sim 2 \text{ kHz}$, $\sim 300 \text{ Hz}$, and $\sim 120 \text{ Hz}$. A detailed description of the detector performance can be found in Di Sciascio et al. (2008) and references therein.

The installation of the whole detector was completed in spring 2007, but since the clusters work independently, physical studies started as the installation began, with the active area

increasing with time. Although the single particle technique does not provide information about the energy and arrival direction of the primary gamma rays, it allows the energy threshold to be lowered to ~ 1 GeV, thus overlapping the highest energies investigated by satellite experiments. Moreover, in our application of this technique to the ARGO-YBJ experiment (Aielli et al. 2008), with four measurement channels sensitive to different energies, in case of positive detection valuable information on the high energy spectrum slope and possible cutoff may be obtained.

Since for the GRB search in scaler mode the authentication is only given by the satellite detection, the stability of the detector and the probability that it mimics a true signal are crucial and have to be carefully investigated. Details of this study are in Aielli et al. (2008), together with the determination of the effective area, upper limit calculation, and expected sensitivity. The results obtained show that the main influences on the counting rates are given by the atmospheric pressure (barometric coefficient for modulation: $-(0.9 - 1.2) \% \text{ mbar}^{-1}$, connected to the shower development in the atmosphere) and the detector temperature (thermal coefficient: $0.2 - 0.4\% \text{ } ^\circ\text{C}^{-1}$, linked to the detector efficiency). Due to the larger time scale variations for these two parameters with respect to the GRB prompt phase duration, the search for GRBs can be carried out without any correction for environmental or instrumental effects, since the relevant distributions for single clusters are Poissonian. More significant is the correlation between the clusters due to the probability that some of the counts in different clusters are given by the same events: the effect in this case is to widen background fluctuations, reducing the sensitivity.

The GRB search can be performed in both shower and scaler modes; in this paper only the results obtained with the latter are presented and discussed.

3. GRB SEARCH

Data have been collected from 2004 November (corresponding to the Swift satellite launch) to 2009 April, with a detector active area increasing from ~ 700 to ~ 6700 m². During this period, a total of 81 GRBs selected from the GCN Circulars Archive¹ was inside the ARGO-YBJ field of view (i.e. with zenith angle $\theta \leq 45^\circ$, limited only by the atmospheric absorption); for 19 of these the detector and/or data acquisition were not active or not working properly. The remaining 62 events were investigated by searching for a significant excess in the ARGO-YBJ data coincident with the satellite detection. In order to extract the maximum information from the data, two GRB analyses have been implemented:

- search for a signal from every single GRB;
- search for a signal from the stack of all GRBs.

For both analyses, the first step is the data cleaning and check. For each event, the Poissonian behaviour of the counting rates for multiplicities ≥ 1 , ≥ 2 , ≥ 3 , ≥ 4 for all the clusters is checked using the normalized fluctuation function:

$$f = (s - b)/\sigma, \quad \sigma = \sqrt{b + b/20} \tag{1}$$

for a period of ± 12 h around the GRB trigger time. In this formula, representing the significance of an excess compared to background fluctuations, s is the number of counts in a time interval of 10 s, b the average number of counts in 10 s over a time period of 100 s before and after the signal, and σ the standard deviation, with about 400 independent samples per distribution. The interval of 10 s has been chosen to avoid any systematic

¹http://gcn.gsfc.nasa.gov/gcn3_archive.html

effect caused by environment and instrument (such as atmospheric pressure and detector temperature variations). The expected distribution of f is the standard normal function; all the clusters giving a distribution with measured $\sigma > 1.2$ or with anomalous excesses in the tail $\sigma > 3$ (i.e. $> 2\%$) in at least one multiplicity channel are discarded. This guarantees that our data fulfill the requirements on stability and reliability of the detector. The counting rates of the clusters surviving our quality cuts ($\sim 87\%$) are then added up and the normalized fluctuation function

$$f' = (s' - b')/\sigma', \quad \sigma' = \sqrt{b' + b' \frac{\Delta t_{90}[s]}{600}} \quad (2)$$

is used to give the significance of the coincident on-source counts. In this case s' is the total number of counts in the Δt_{90} time interval given by the satellite detector (corresponding to the collection of 90% of the photons) and b' is the number of counts in a fixed time interval of 300 s before and after the signal, normalized to the Δt_{90} time. Due to the correlation between the counting rates of different clusters (given by the air shower lateral distribution), the distributions of the sum of the counts are larger than Poissonian and this must be taken into account to calculate the significance of a possible signal. The statistical significance of the on-source counts over the background is obtained again in an interval of ± 12 h around the GRB trigger time, using equation (17) of Li & Ma (1983); a detailed analysis of the correlation effect and detector stability on counting rates can be found in Aielli et al. (2008). The analysis can be carried out for the counting rates for all the multiplicities $\geq 1, \geq 2, \geq 3, \geq 4$, and 1, 2, 3, where the counting rates C_i are obtained from the measured counting rates $C_{\geq i}$ using the relation:

$$C_i = C_{\geq i} - C_{\geq i+1} \quad (i = 1, 2, 3) \quad (3)$$

As an example, figure 1 shows the $f'(C_1)$ distribution for a single cluster and for the sum of all clusters for GRB060121; even if all the single clusters show a Poissonian behaviour, with width $\sigma \sim 1$, the correlation effect on the sum of the counting rates of all clusters broadens the $f'(\sum C_{1,i})$ distribution ($\sigma > 1$). In the following, all the results are obtained using the counting rate C_1 , since it corresponds to the minimum primary energy in the ARGO-YBJ scaler mode. Figure 2 shows the distribution of the significances for the whole set of 62 GRBs. The Gaussian fit to this distribution gives a mean of $(-0.01 \pm 0.16)\sigma$ and standard deviation (1.22 ± 0.14) . No significant excess is shown; the maximum significance is obtained for GRB080727C (3.52σ), with a chance probability of 1.4% taking into account the total number of GRBs analyzed.

The fluence upper limits are then obtained in the 1-100 GeV energy range adopting a power law spectrum and considering the maximum number of counts at 99% confidence level (c.l.), following equation (6) of Helene (1983). For this calculation, two different assumptions are used for the power law spectrum: a) extrapolation from the keV-MeV energy region using the spectral index measured by the satellite experiments; b) a differential spectral index $\alpha = -2.5$. Since the mean value of spectral indexes measured by EGRET in the GeV energy region is $\alpha = -2.0$ (Dingus et al. 1997), we expect the true upper limits to lie between these two values. For GRBs with known redshift, an exponential cutoff in the spectrum is considered in order to take into account the effects of extragalactic absorption. The extinction coefficient is calculated using the values given in Kneiske et al. (2004). When the redshift is unknown, a value $z = 1$ is adopted.

Since the cutoff energy of GRBs is unknown, the following procedure is developed in order to determine an upper limit to this energy at least for some GRBs. When using as the GRB spectrum the extrapolation of the spectral index measured in the keV-MeV region by satellite experiments, the extrapolated fluence is plotted together with our fluence upper limit as a function of the cutoff energy E_{cut} . If the two curves cross in the 2-100 GeV

energy range, the intersection gives the upper limit to the cutoff energy. For these GRBs we can state that their spectra do not extend over the obtained E_{cut} upper limit, with a 99% c.l.. Figure 3 shows the cutoff energy upper limits as a function of the spectral index for the 16 GRBs for which intersection occurs in the quoted energy range. For two of them (GRB050802 and GRB081028A) the knowledge of the redshift allows the estimation of extragalactic absorption.

Table 1 lists all the information related to the 9 GRBs with known redshift; Table 2 lists the same information for the remaining 53 GRBs. In both tables column (1) is the GRB name corresponding to the detection date in UT (YYMMDD). Column (2) gives the satellite(s) that detected the burst. Column (3) gives the burst duration Δt_{90} as measured by the respective satellite. Column (4) gives the zenith angle in degrees with respect to the detector location. Column (5) reports the spectral index: “Band” and “CPL” mean that the spectrum measured by the satellite is better fitted with a double power law (Band et al. 1993) or a Cutoff Power Law, respectively. In this latter case no extrapolation of the spectrum to GeV energies has been considered. Column (6) gives the detector active area for that burst. Our results are reported from column (7) to (10). Column (7) gives the statistical significance of the on-source counts over the background; columns (8) and (9) the 99% confidence upper limits on the fluence between 1 and 100 GeV for spectral cases a) and b), respectively; column (10) the cutoff energy upper limit, if any. The additional column (11) in Table 1 gives the GRB redshift.

The fluence upper limits obtained in the 1-100 GeV energy range depend on the zenith angle, time duration and spectral index, reaching values down to 10^{-5} erg cm $^{-2}$. It is worth noticing that these values greatly depend on the energy range of the calculation. If we consider our sensitivity in terms of the expected number of positive detections, an estimate based on data from the satellite CGRO and the Swift field of view gives a rate between 0.1 and 0.5 per year (Aielli et al. 2008), which is comparable to similar evaluations for other

experiments working in different energy regions (e.g. Albert et al. 2007).

A different analysis is performed supposing a common timing feature in all the GRBs.

First, all the events during a time interval Δt (with $\Delta t=0.5, 1, 2, 5, 10, 20, 50, 100, 200$ s) after T_0 (the low energy trigger time given by the satellite) for all the GRBs are added up. This is done in order to search for a possible cumulative high energy emission with a fixed duration after T_0 . The resulting significances for the 9 time bins (figure 4) show that there is no evidence of emission for any one of the durations Δt . Since the bins are not independent, the distribution of the significances of the 9 time bins is compared with random distributions obtained for starting times different from T_0 in a time interval of ± 12 h around the true GRB trigger time. The resulting overall significance of the GRBs stacked in time with respect to random fluctuations is -0.6σ . A second search is carried out to test the hypothesis that the high energy emission occurs at a specific phase of the low energy burst, independently of the GRB duration. For this study, all 53 GRBs with $\Delta t_{90} \geq 5$ s (i.e. belonging to the “long GRB” population) have been added up in phase scaling their duration. This choice has been made for both physical and technical reasons, adding up the counts for GRBs of the same class and long enough to allow a phase plot with 10 bins given our time resolution of 0.5 s. Figure 5 shows the resulting significances for the 10 phase bins; there is no evidence of emission at a certain phase, and the overall significance of the GRBs stacked in phase (obtained adding up all the bins) with respect to background fluctuations is -1.4σ . The search for cumulative effects by stacking all the GRBs either in fixed time durations or in phases of Δt_{90} could enhance a possible signal, making it significant, even if the emission of each GRB is below the sensitivity of the ARGO-YBJ detector. In this case, less information could be given with respect to the single GRB coincident detection, but we must consider that with the stacked analysis we increase our sensitivity by increasing the number of GRBs, while for the single GRB search we decrease our sensitivity because of the increasing number of trials.

4. DISCUSSION AND CONCLUSIONS

The satellite-borne detectors have detected GRBs mostly in the sub-MeV energy region. However, several GRBs with emission beyond 100 MeV have been detected by EGRET (Schneid et al. 1992; Hurley et al. 1994; Catelli et al. 1997) and, recently, by AGILE (Giuliani et al. 2008) and by the LAT instrument on the Fermi Gamma Ray Space Telescope (Tajima et al. 2008). These detections indicate that at least a fraction of GRBs, in addition to sub-MeV photons, may also emit much higher energy photons, possibly extending to the GeV-TeV region. Within the standard fireball shock scenario, high energy photons can be produced in both internal (Paczynski & Xu 1994; Mészáros & Rees 1994) and external (Rees & Mészáros 1992) shocks, either by the electron component through the inverse Compton process or by the proton component through synchrotron or photo-pion processes. Due to the interaction with cosmic infrared background photons, most of the high energy GRB photons are converted into electron-positron pairs, thus limiting the distance over which they can travel. A correlated detection of GRB high energy photons, associated to the redshift measurement based on spectroscopic observations, could help determine the extension of the gamma ray horizon and shed light on the problem of the universe “transparency” recently raised by the observations of the HESS (Aharonian et al. 2006) and MAGIC (Albert et al. 2008) telescopes. Proposed explanations of these observations refer to models for the EBL evolution (Stecker et al. 2006; Stecker & Scully 2009) as well as the particle physics process of photon-ALP (Axion-Like Particle) oscillation (Sikivie 1983; De Angelis et al. 2008). Thus, the observation of GRB high energy photons is expected to provide important information both on the physical conditions of the emission region and on the interaction processes undergone by the photons while traveling from the source. In this paper we have reported a study concerning the search for GeV photons from 62 GRBs carried out by the ARGO-YBJ air shower detector operated in scaler mode. In the search for GeV gamma rays in coincidence with the low energy GRBs detected by satellites,

no evidence for VHE emission was found for any event. The stacked search, both in time and phase, has shown no deviation from the statistical expectations.

Fluence upper limits as low as $\lesssim 10^{-5}$ erg cm $^{-2}$ in the 1 – 100 GeV interval have been set by using ARGO-YBJ data. Using the experimental values obtained for the GRBs with known redshift and $\alpha = -2.5$, we have calculated the corresponding minimum isotropic gamma ray energy E_{iso} . Considering a cosmology with Hubble constant $H_0 = 70$ km s $^{-1}$ Mpc $^{-1}$, matter and dark energy density parameters $\Omega_m = 0.3$ and $\Omega_\Lambda = 0.7$, respectively (Komatsu et al. 2008), we find the minimum value $E_{iso} = 2.5 \times 10^{53}$ erg for GRB071112C, emitted in the energy band 1.8 – 180 GeV due to its redshift $z=0.823$. This value is quite high, compared to the expected maximum bolometric isotropic energy of about 10^{54} erg, but a beaming effect depending on the energy could greatly change the fraction of the total energy amount required in the quoted energy range.

Some relevant constraints can be obtained comparing our fluence upper limits with the expected theoretical spectra. Under different assumptions, the model of Asano & Inoue (2007) predicts GRB spectra at $z=0.1$ with fluences (in terms of $E \times F(E)$) roughly between 2×10^{-5} and 2×10^{-4} erg cm $^{-2}$ in our energy range of interest. Considering the same cosmological parameters as above and the minimum fluence upper limit of 8.1×10^{-6} erg cm $^{-2}$ (corresponding to GRB060801), the maximum redshift at which such a GRB could be detected by ARGO-YBJ ranges between $z = 0.3$ and 1.0.

Since we were able to determine upper limits to the cutoff energy in the 2 – 100 GeV energy range for several GRBs, we can conclude that a simple extension of the power law spectra measured at low energies is not always possible (Band et al. 1993).

Finally, the alert rate provided by the recently launched Fermi satellite, with a field of view close to that of Swift, doubles our estimate of GRB detection (Aielli et al. 2008) up to a rate between 0.2 and 1 per year, and the capability of the detector shower mode to measure the arrival direction and energy of individual showers above a few hundred GeV allows the

ARGO-YBJ experiment to study the GRBs in the whole 1 GeV–1 TeV range.

This paper is supported in part by the National Natural Science Foundation of China (NSFC) under the grant No. 10120130794, the Chinese Ministry of Science and Technology, the Key Laboratory of Particle Astrophysics, Institute of High Energy Physics (IHEP), Chinese Academy of Science (CAS), and the National Institute of Nuclear Physics of Italy (INFN).

M. Dattoli thanks the National Institute of Astrophysics of Italy (INAF) for partly supporting her activity in this work.

REFERENCES

- Aharonian, F., et al. 2006, *Nature*, 440, 1018.
- Aielli, G., et al. 2006, *Nuclear Instruments and Methods*, A562, 92.
- Aielli, G., et al. 2008, *Astroparticle Physics*, 30, 85.
- Albert, J., et al. 2007, *ApJ*, 667, 358.
- Albert, J., et al. 2008, *Science*, 320, 1752.
- Amenomori, M., et al. 1996, *A&A*, 311, 919.
- Asano, K., & Inoue, S. 2007, *ApJ*, 671, 645.
- Atkins, R., et al. 2000, *ApJ*, 533, L119.
- Band, D., et al. 1993, *ApJ*, 413, 281.
- Catelli, J.R., Dingus, B.L., & Schneid, E.J. 1997, in *Gamma Ray Bursts*, AIP Conf. Proc. No. 428, ed. C.A. Meegan (AIP, New York), 309.
- Costa, E., et al. 1997, *Nature*, 387, 783.
- De Angelis, A., Mansutti, O., Persic, M., & Roncadelli, M. 2008, arXiv:0807.4246, *MNRAS Letters*, in press.
- Di Sciascio, G., & the ARGO-YBJ Collaboration 2008, arXiv:0811.0997, *Proceedings of the Vulcano Workshop 2008*, in press.
- Dingus, B.L., Catelli, J.R., & Schneid, E.J. 1997, in *Proceedings of the 25th ICRC*, 3, 29.
- Fox, D.B., & Mészáros, P. 2006, *New Journal of Physics*, 8, 199.
- Giuliani, A., et al. 2008, *A&A*, 491, L25.

- Helene, O. 1983, *Nuclear Instruments and Methods*, 212, 319.
- Hurley, K., et al. 1994, *Nature*, 372, 652.
- Kneiske, T.M., Bretz, T., Mannheim, K., & Hartmann, D.H. 2004, *A&A*, 413, 807.
- Komatsu, E., et al. 2008, arXiv:0803.0547, *ApJS*, in press.
- Li, T., & Ma, Y. 1983, *ApJ*, 272, 317.
- Mészáros, P., & Rees, M.J. 1994, *Monthly Notices of the Royal Astronomical Society*, 269, L41.
- Mészáros, P. 2006, *Reports on Progress in Physics*, 69, 2259.
- Omodei, N., & the Fermi-LAT Collaboration 2008, *GCN Circular*, 8407.
- Paczyński, B., & Xu, G. 1994, *ApJ*, 427, 708.
- Padilla, L., et al. 1998, *A&A*, 337, 43.
- Poirier, J., D’Andrea, C., Fragile, P.C., Gress, J., Mathews, G.J., & Race, D. 2003, *Physical Review D*, 67, 042001.
- Rees, M.J., & Mészáros, P. 1992, *Monthly Notices of the Royal Astronomical Society*, 258, P41.
- Salamon, M.H., & Stecker, F.W. 1998, *ApJ*, 493, 547.
- Schneid, E.J., et al. 1992, *A&A*, 255, L13.
- Sikivie, P. 1983, *Physical Review Letters*, 51, 1415 [Erratum-ibid. 1984, 52, 695].
- Stecker, F.W., Malkan, M.A., & Scully, S.T. 2006, *ApJ*, 648, 774.
- Stecker, F.W., & Scully, S.T. 2009, *ApJL*, 691, L91.

Tajima, H., Bregeon, J., Chiang, J., Thayer, G., & the Fermi-LAT team 2008, GCN Circular, 8246.

Totani, T. 2000, ApJL, 536, L23.

Vernetto, S. 2000, Astroparticle Physics, 13, 75.

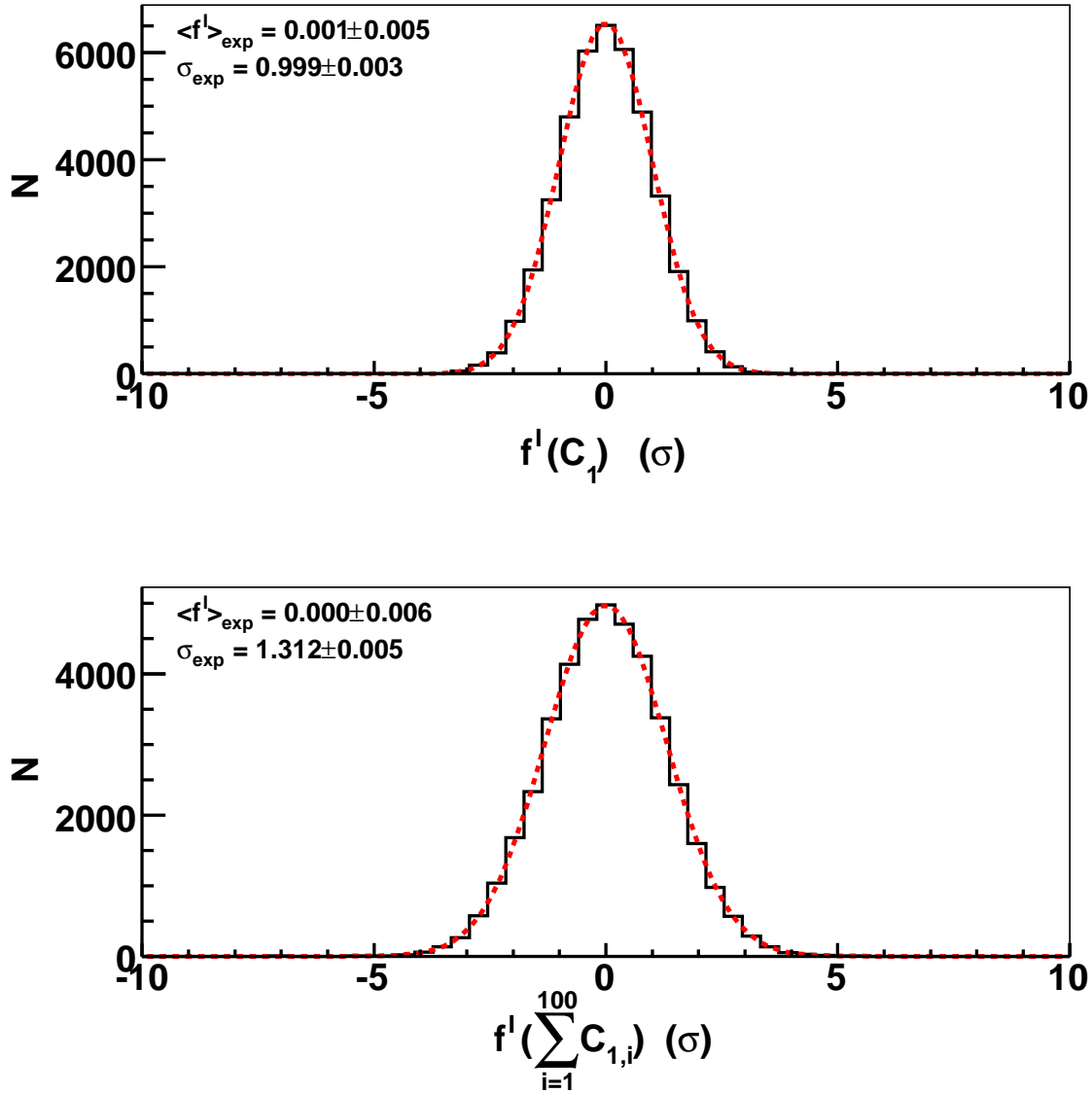


Fig. 1.— Experimental distribution of the normalized excesses of signal over background for GRB060121. Top: C_1 channel for a typical cluster compared with a Gaussian fit; bottom: sum of the 100 active clusters.

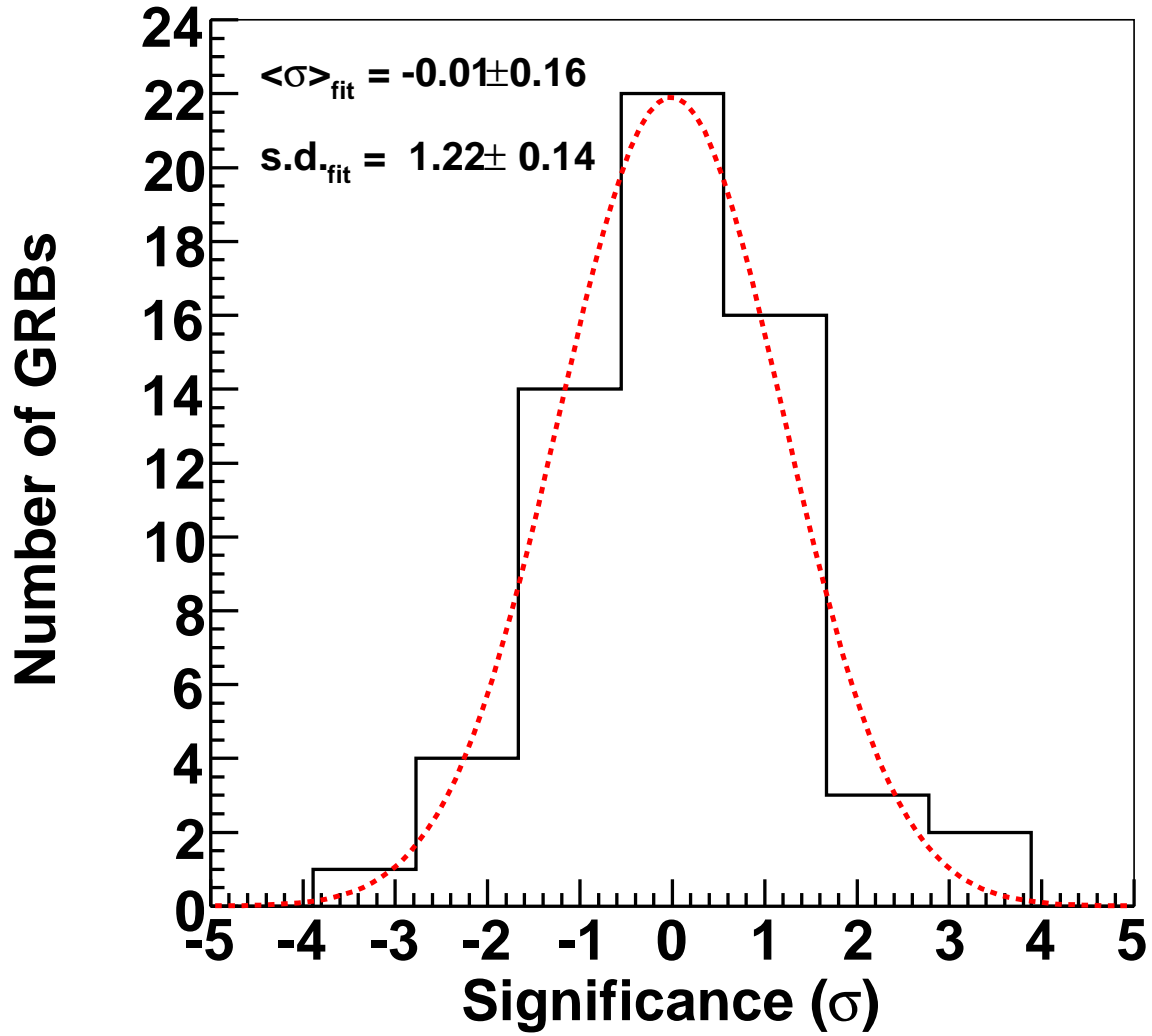


Fig. 2.— Distribution of the statistical significances of the 62 GRBs with respect to background fluctuations, compared with a Gaussian fit.

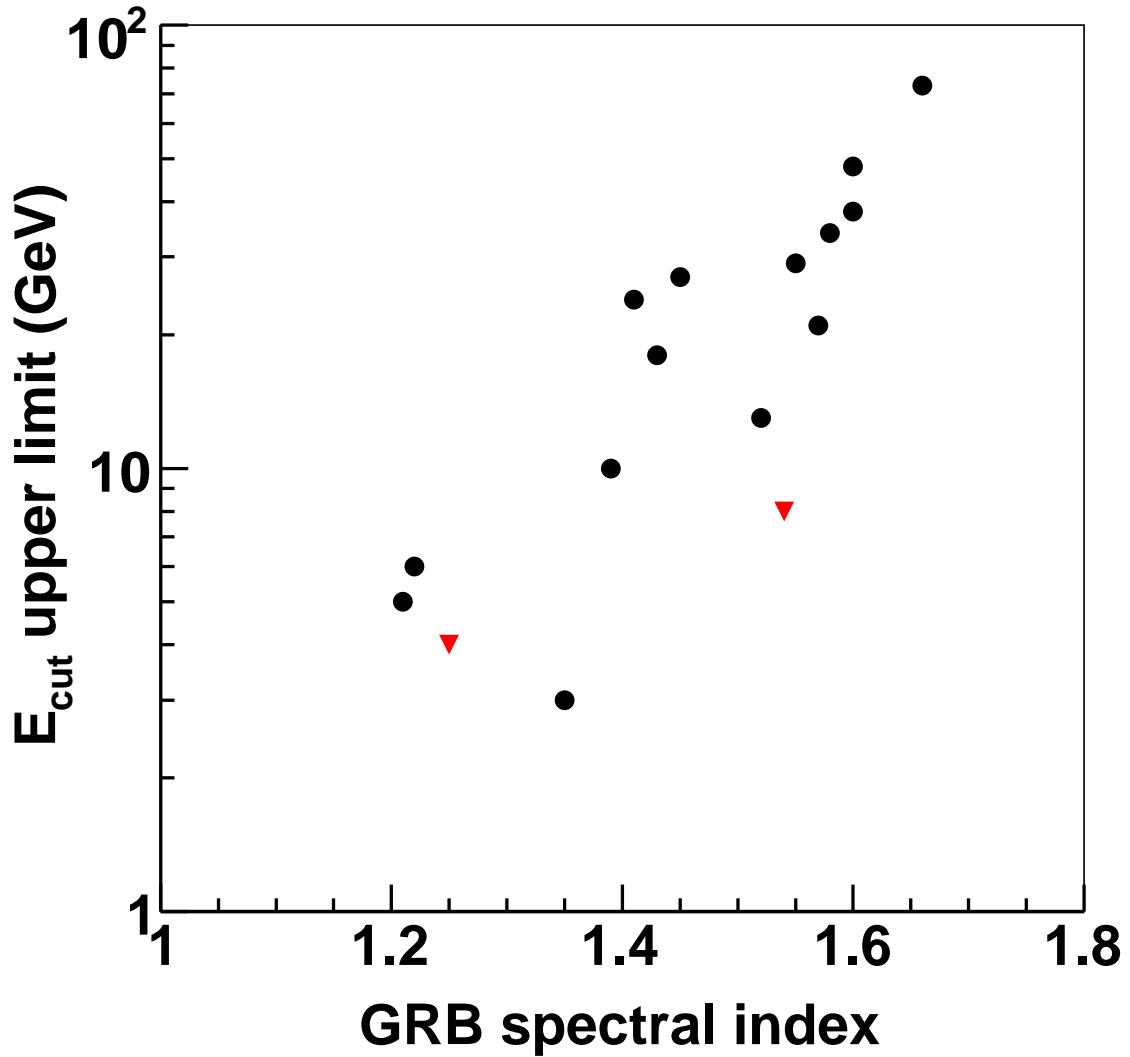


Fig. 3.— Cutoff energy upper limits as a function of the spectral index obtained by extrapolating the measured keV spectra. The values represented by the triangles are obtained taking into account extragalactic absorption.

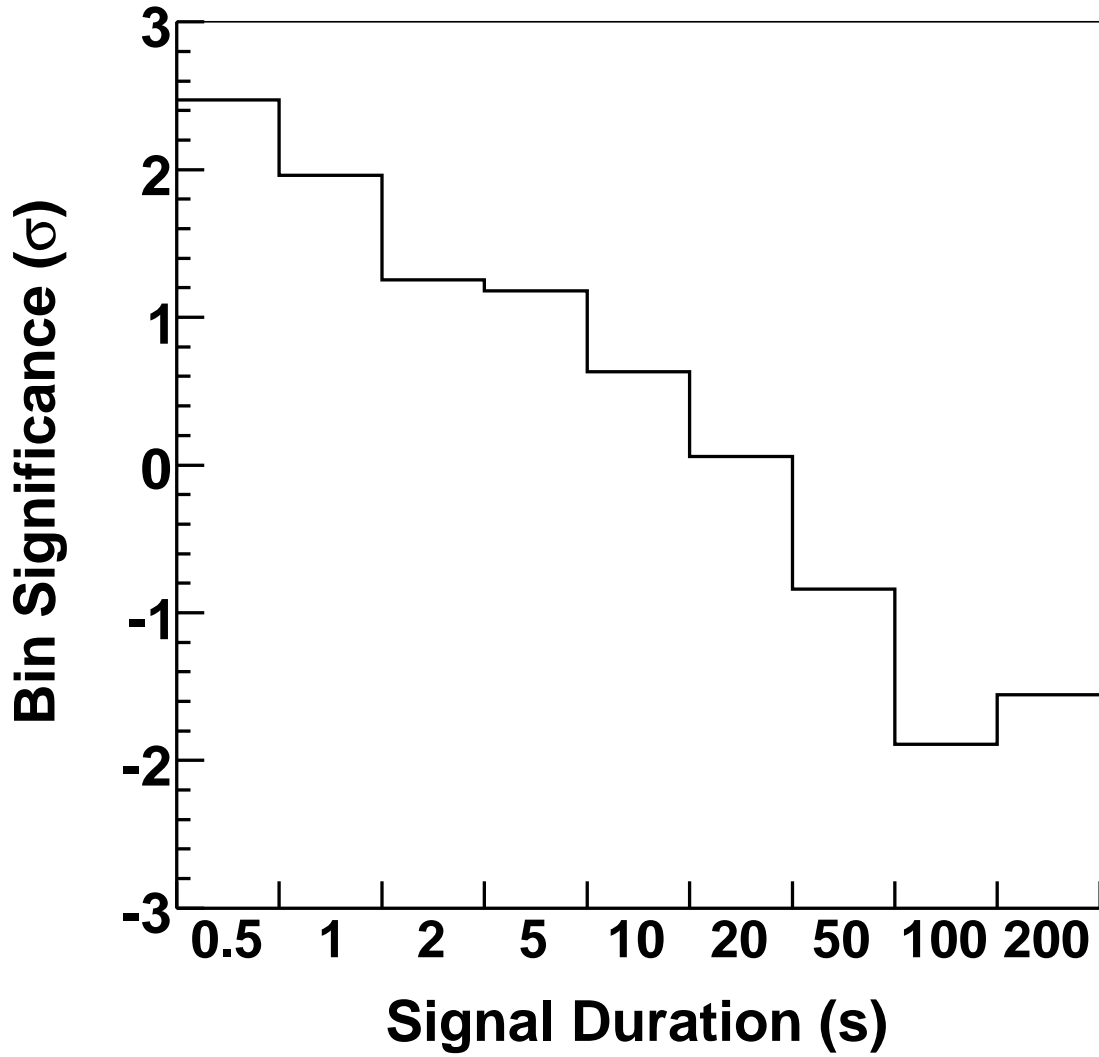


Fig. 4.— Significances of GRBs stacked in time for durations between 0.5 and 200 s after the low energy trigger time T_0 .

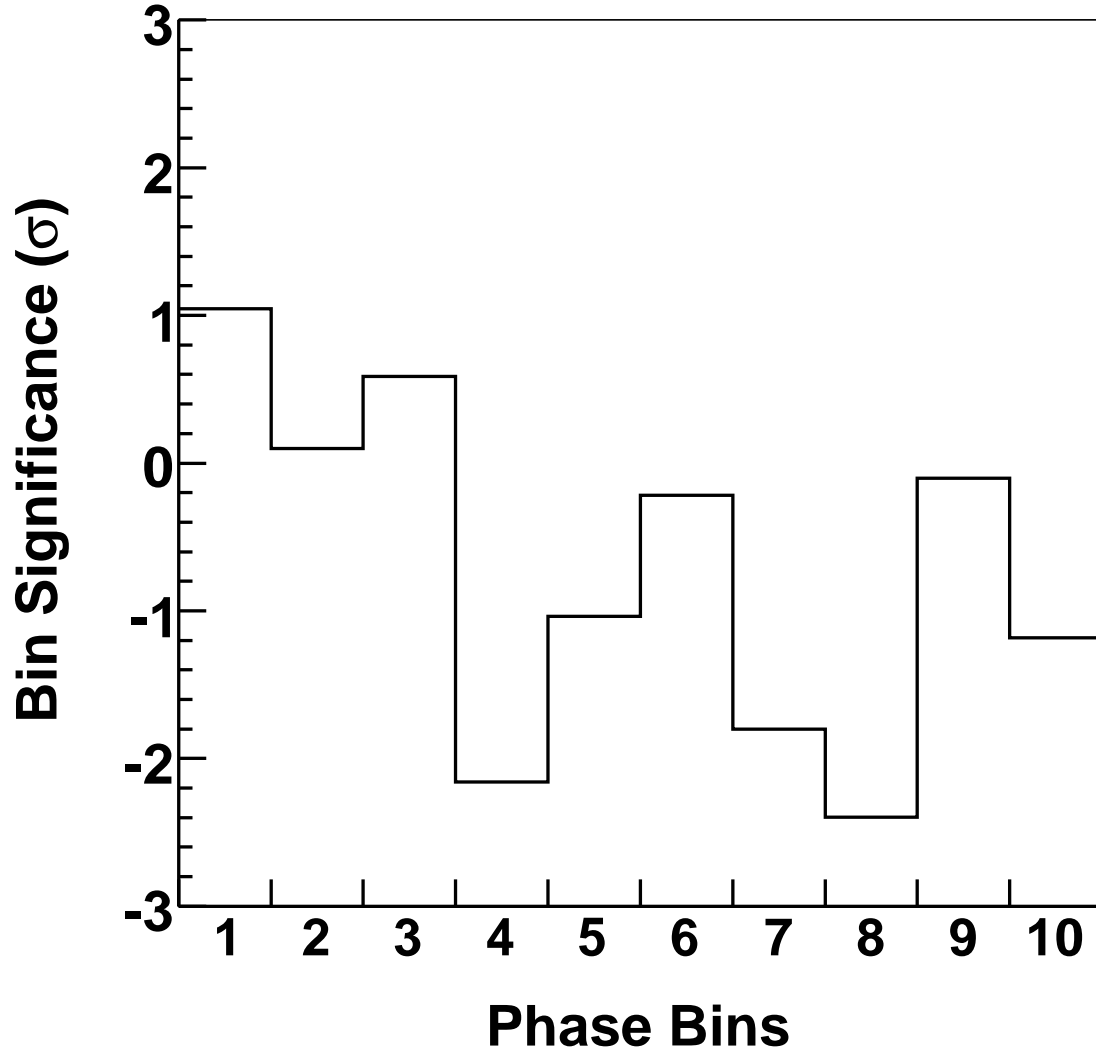


Fig. 5.— Significances of GRBs with duration $\Delta t_{90} \geq 5s$ stacked in phase (see text).

Table 1. GRBs with Measured Redshift Observed by ARGO-YBJ.

GRB (1)	Satellite (2)	Δt_{90} (s) (3)	$\theta(^{\circ})$ (4)	Spectral Index (5)	A_{det} (m ²) (6)	σ (7)	Fluence U.L. (erg cm ⁻²) ^{a,c} (8)	Fluence U.L. (erg cm ⁻²) ^{b,c} (9)	E_{cut} U.L. (GeV) ^c (10)	Redshift z (11)
050408	HETE	15	20.4	CPL ^d	1560	-2.12	–	9.1×10^{-5}	–	1.24
050802	Swift	19.0	22.5	1.54	1516	0.19	1.0×10^{-4}	2.1×10^{-4}	8	1.71
060115	Swift	139.6	16.6	CPL ^d	3985	-1.02	–	7.6×10^{-4}	–	3.53
060526	Swift	298.2	31.7	2.01	4029	-1.00	1.8×10^{-3}	2.7×10^{-3}	–	3.21
060714	Swift	115.0	42.8	1.93	5155	-0.61	4.2×10^{-3}	6.9×10^{-3}	–	2.71
060927	Swift	22.5	31.6	CPL ^d	5242	-0.14	–	5.1×10^{-4}	–	5.6
061110A	Swift	40.7	37.3	1.67	5545	0.01	6.7×10^{-4}	1.7×10^{-3}	–	0.76
071112C	Swift	15	18.4	1.09	5198	1.01	4.5×10^{-5}	1.4×10^{-4}	< 2	0.823
081028A	Swift	260	29.9	1.25	5805	0.37	1.1×10^{-3}	3.0×10^{-3}	4	3.028

Note. — ^aUsing the spectrum determined by satellites. ^bAssuming a differential spectral index 2.5. ^c99% c.l.. ^dSee text.

Table 2. GRBs with no Redshift ($z = 1$ is assumed) Observed by ARGO-YBJ.

GRB (1)	Satellite (2)	Δt_{90} (s) (3)	$\theta(^{\circ})$ (4)	Spectral Index (5)	A_{det} (m ²) (6)	σ (7)	Fluence U.L. (erg cm ⁻²) ^{a,c} (8)	Fluence U.L. (erg cm ⁻²) ^{b,c} (9)	E_{cut} U.L. (GeV) ^c (10)
041228	Swift	55.4	28.1	1.60	563	-0.01	4.4×10^{-4}	1.1×10^{-3}	38
050509A	Swift	11.4	34.0	2.11	1473	0.62	1.9×10^{-4}	3.0×10^{-4}	–
050528	Swift	11.3	37.8	2.27	1473	0.71	8.0×10^{-4}	1.0×10^{-3}	–
051105A	Swift	0.1	28.5	1.22	3119	1.24	1.6×10^{-5}	4.8×10^{-5}	6
051114	Swift	2.2	32.8	1.21	3032	3.37	5.6×10^{-5}	1.8×10^{-4}	5
051227	Swift	114.6	22.8	1.45	2989	0.44	3.7×10^{-4}	9.2×10^{-4}	27
060105	Swift	54.4	16.3	1.07	3119	1.77	2.5×10^{-4}	7.7×10^{-4}	< 2
060111A	Swift	13.2	10.8	CPL ^d	3206	0.39	–	9.7×10^{-5}	–
060121	HETE	2.0	41.9	Band ^d	4159	0.60	2.5×10^{-4}	2.8×10^{-4}	–
060421	Swift	12.2	39.3	1.55	3855	-0.51	2.0×10^{-4}	5.2×10^{-4}	29
060424	Swift	37.5	6.7	1.71	4072	0.12	7.5×10^{-5}	1.6×10^{-4}	–
060427	Swift	64.0	32.6	1.87	4115	-0.13	2.6×10^{-4}	5.1×10^{-4}	–
060510A	Swift	20.4	37.4	1.57	3899	2.42	6.8×10^{-4}	1.8×10^{-3}	21
060717	Swift	3.0	7.4	1.70	5155	1.58	2.3×10^{-5}	4.8×10^{-5}	–
060801	Swift	0.5	16.8	0.47	5415	0.81	8.1×10^{-6}	3.0×10^{-5}	< 2
060805B	IPN	8	29.1	Band ^d	5285	-0.45	1.2×10^{-4}	1.1×10^{-4}	–
060807	Swift	54.0	12.4	1.58	5155	0.78	1.3×10^{-4}	3.0×10^{-4}	34
061028	Swift	106.2	42.5	1.73	5458	-3.33	3.5×10^{-4}	8.0×10^{-4}	–
061122	INTEGRAL	18	33.5	CPL ^d	5025	0.60	–	6.4×10^{-4}	–
070201	IPN	0.3	20.6	CPL ^d	5242	-1.21	–	1.2×10^{-5}	–
070219	Swift	16.6	39.3	1.78	4982	-0.71	3.1×10^{-4}	6.8×10^{-4}	–
070306	Swift	209.5	19.9	1.66	2513	-0.83	5.4×10^{-4}	1.2×10^{-3}	73
070531	Swift	44.5	44.3	1.41	2816	0.59	6.6×10^{-4}	1.9×10^{-3}	24

Table 2—Continued

GRB	Satellite	Δt_{90} (s)	θ ($^\circ$)	Spectral Index	A_{det} (m ²)	σ	Fluence U.L. (erg cm ⁻²) ^{a,c}	Fluence U.L. (erg cm ⁻²) ^{b,c}	E_{cut} U.L. (GeV) ^c
(1)	(2)	(3)	(4)	(5)	(6)	(7)	(8)	(9)	(10)
070615	IINTEGRAL	30	37.6	–	5328	1.81	–	1.7×10^{-3}	–
071013	Swift	26	13.3	1.60	4765	-0.06	5.2×10^{-5}	1.2×10^{-4}	48
071101	Swift	9.0	32.8	2.25	3596	1.01	1.6×10^{-4}	2.1×10^{-4}	–
071104	AGILE	12	19.9	–	4029	-0.07	–	1.3×10^{-4}	–
071118	Swift	71	41.2	1.63	5025	0.54	1.3×10^{-3}	3.3×10^{-3}	–
080328	Swift	90.6	37.2	1.52	6065	-1.19	7.6×10^{-4}	2.1×10^{-3}	13
080602	Swift	74	42.0	1.43	5762	1.24	1.1×10^{-3}	3.1×10^{-3}	18
080613B	Swift	105	39.2	1.39	5718	0.65	1.2×10^{-3}	3.6×10^{-3}	10
080727C	Swift	79.7	34.5	CPL ^d	5415	3.52	–	1.4×10^{-3}	–
080822B	Swift	64	40.3	2.54	5762	-1.84	1.3×10^{-3}	1.3×10^{-3}	–
080830	Fermi	45	37.1	Band ^d	5805	-0.04	6.3×10^{-4}	1.5×10^{-3}	–
080903	Swift	66	21.5	CPL ^d	5588	-1.33	–	2.3×10^{-4}	–
081025	Swift	23	30.5	1.12	5718	-0.48	6.0×10^{-5}	2.0×10^{-4}	< 2
081102B	Fermi	2.2	27.8	1.07	5762	0.02	1.7×10^{-5}	5.8×10^{-5}	< 2
081105	IPN	10	36.7	–	5718	-0.77	–	4.0×10^{-4}	–
081122	Fermi	26	8.3	Band ^d	4289	-2.03	5.5×10^{-5}	7.1×10^{-5}	–
081128	Swift	100	31.8	CPL ^d	5242	-0.63	–	9.8×10^{-4}	–
081130B	Fermi	12	28.6	CPL ^d	5978	-0.05	–	2.2×10^{-4}	–
081215A	Fermi	7.7	35.9	Band ^d	5762	-0.15	3.1×10^{-4}	5.1×10^{-4}	–
090107A	Swift	12.2	40.1	1.69	5762	-1.12	2.2×10^{-4}	5.3×10^{-4}	–
090118	Swift	16	13.4	1.35	5805	-1.62	2.1×10^{-5}	5.5×10^{-5}	3
090126B	Fermi	10.8	3.7	CPL ^d	5892	-1.43	–	4.0×10^{-5}	–
090227B	Fermi	0.9	9.7	CPL ^d	5935	0.21	–	1.6×10^{-5}	–

Table 2—Continued

GRB	Satellite	Δt_{90} (s)	$\theta(^{\circ})$	Spectral Index	A_{det} (m ²)	σ	Fluence U.L. (erg cm ⁻²) ^{a,c}	Fluence U.L. (erg cm ⁻²) ^{b,c}	E_{cut} U.L. (GeV) ^c
(1)	(2)	(3)	(4)	(5)	(6)	(7)	(8)	(9)	(10)
090301	Swift	41.0	14.2	CPL ^d	5805	0.73	–	2.3×10^{-4}	–
090301B	Fermi	28	24.3	Band ^d	5892	-2.20	6.2×10^{-5}	1.1×10^{-4}	–
090306B	Swift	20.4	38.5	CPL ^d	5805	-0.65	–	9.3×10^{-4}	–
090320B	Fermi	52	29.0	CPL ^d	5892	-0.25	–	2.4×10^{-4}	–
090328B	Fermi	0.32	15.5	Band ^d	5848	0.48	1.7×10^{-5}	1.8×10^{-5}	–
090403	Fermi	16	28.5	–	6021	0.65	–	2.5×10^{-4}	–
090407	Swift	310	45.0	1.73	6021	1.53	5.0×10^{-3}	1.1×10^{-2}	–

Note. — ^aUsing the spectrum determined by satellites. ^bAssuming a differential spectral index 2.5. ^c99% c.l.. ^dSee text.